Self-Propelled Micromotors for Naked-Eye Detection of Phenylenediamines Isomers

Roberto María-Hormigos,† Beatriz Jurado-Sánchez,*,†,‡ and Alberto Escarpa*,†,‡

†Department of Analytical Chemistry, Physical Chemistry and Chemical Engineering, and ‡Chemical Research Institute "Andrés M. del Río", University of Alcala, Alcala de Henares E-28871, Madrid Spain

ABSTRACT: Tubular micromotors composed of a hybrid single-wall carbon nanotube (SW)−Fe_2O_3 outer layer and powered by a MnO_2 catalyst are used for phenylenediamines isomers detection and discrimination. Catalytic decomposition of H_2O_2 as fuel results in the production of oxygen bubbles and hydroxyl radicals for phenylenediamines dimerization to produce colorful solutions in colorimetric assays. The combination of Fe_2O_3 nanoparticles along with the irregular SW backbone results in a rough catalytic layer for enhanced hydroxyl radical production rate and improved analytical sensitivity. Such self-propelled micromotors act as peroxidase-like mobile platforms that offer efficient phenylenediamines detection and discrimination in just 15 min. Factors influencing the colorimetric assay protocol, such as the navigation time and number of motors, have been investigated. Low limits of detection (5 and 6 μM) and quantification (17 and 20 μM) were obtained for o-phenylenediamine and p- phenylenediamine, respectively. The magnetic properties of the outer SW−Fe_2O_3 hybrid layer allow the reusability of the micromotors in the colorimetric assay. Such attractive performance holds considerable promise for its application in sensing systems in a myriad of environmental, industrial, and health applications.

Discrimination and detection of structural isomers constitute an intriguing and challenging task in chemistry, pharmacology, and biology sciences due to its similar skeletons in addition to their similar physical and chemical properties.[1−5] *o*-Phenylenediamine (OPD), *m*-phenylenediamine (MPD), and *p*-phenylenediamine (PPD) are isomers used as chemical intermediates or precursors in the production of plastics, photosensitive materials, and industrial dyes.[6−9] Such isomers exhibit different effects upon human health and the environment. Thus, OPD is a serious environmental pollutant owing to its toxicity and carcinogenicity (LD_{50} = 110 μM). PPD can cause allergic reactions such as acute inflammation or dermatitis.[6,9] Yet, MPD does not cause any apparent harmful effect.

Analytical approaches for isomers detection such as gas or liquid chromatography and capillary electrophoresis[10−14] are expensive and time-consuming. As an alternative, colorimetric (bio)sensing strategies have attracted significant interest owing to their low cost, simplicity, and easy detection with the naked eye.[15] Judicious transformation of analytes such as phenylenediamines into readily detectable colored compounds is the key challenge here. Enzyme-like nanomaterials hold considerable promise as colorimetric tools in several assays.[7] Especially, metal oxide nanoparticles (NPs) have been used as a peroxidase-like catalysts for OH radicals mediated reactions. Fe_3O_4,[9,16] cerium oxide,[17] CuO,[18] Co_3O_4,[19] and MnO_2 NPs[20] have been employed as horseradish peroxidase (HRP) enzyme mimics for classical HRP substrates, i.e., 3,3′,5,5′-tetramethylbenzidine or 2,2′-azino-bis(3-ethylbenzothiazoline-6-sulfonate). However, free nanoparticles are highly unstable in solution because they are prone to agglomeration, which results in the loss of their catalytic activity.[21] To overcome these problems, a variety of supports including carbon nanomaterials and conducting polymers have been employed to maximize their stability and catalytic activity.[21]

Catalytic micromotors hold considerable promise not only as supports for catalysts but also as self-propelled devices with intrinsic peroxidase-like activity and solution mixing.[22−33] Receptor-functionalized or quantum dots modified micromotors have been successfully applied for the isolation or detection of biological targets,[34] toxins,[35−37] or heavy metals.[38] Magnesium-based Janus micromotors display enzyme-like activity, which has been exploited for the electrochemical detection of non-electroactive paraoxon[39] or diphenyl phthalate.[40] The binomium carbon allotrope nanomaterial−metal oxide catalysts represent a convenient strategy to improve the performance of micromotors toward enhanced peroxidase activity.[41−44] The use of MnO_2 or Ag to replace Pt as the catalytic unit allows for reducing overall cost in practical applications.[45−47] Alternative propulsion mechanisms such as magnetic fields can also eliminate the requirements for expensive catalysts.[48] Herein we describe the synthesis of single-wall carbon nanotube (SW)−Fe_2O_3/MnO_2 micromotors for phenylenediamine isomers discrimination and detection in water samples. Micromotors are prepared by template electrodeposition involving the simultaneous deposition of a first hybrid SW layer containing "trapped" Fe_2O_3 nanoparticles, followed by the deposition of a second inner MnO_2 catalytic layer. As will be also illustrated, such an outer layer imparts the micromotors with magnetic properties for further reusability. Decomposition of H_2O_2 fuel results in the production of oxygen bubbles along with hydroxyl radicals for further dimerization of phenylenediamines into a characteristic-colored compounds (see **Figure 1**). Enhanced micromotor movement along with radical generation results in rapid assays for OPD, MPD, and PPD detection in just 15 min with enough sensitivity for colorimetric "naked eye" schemes.

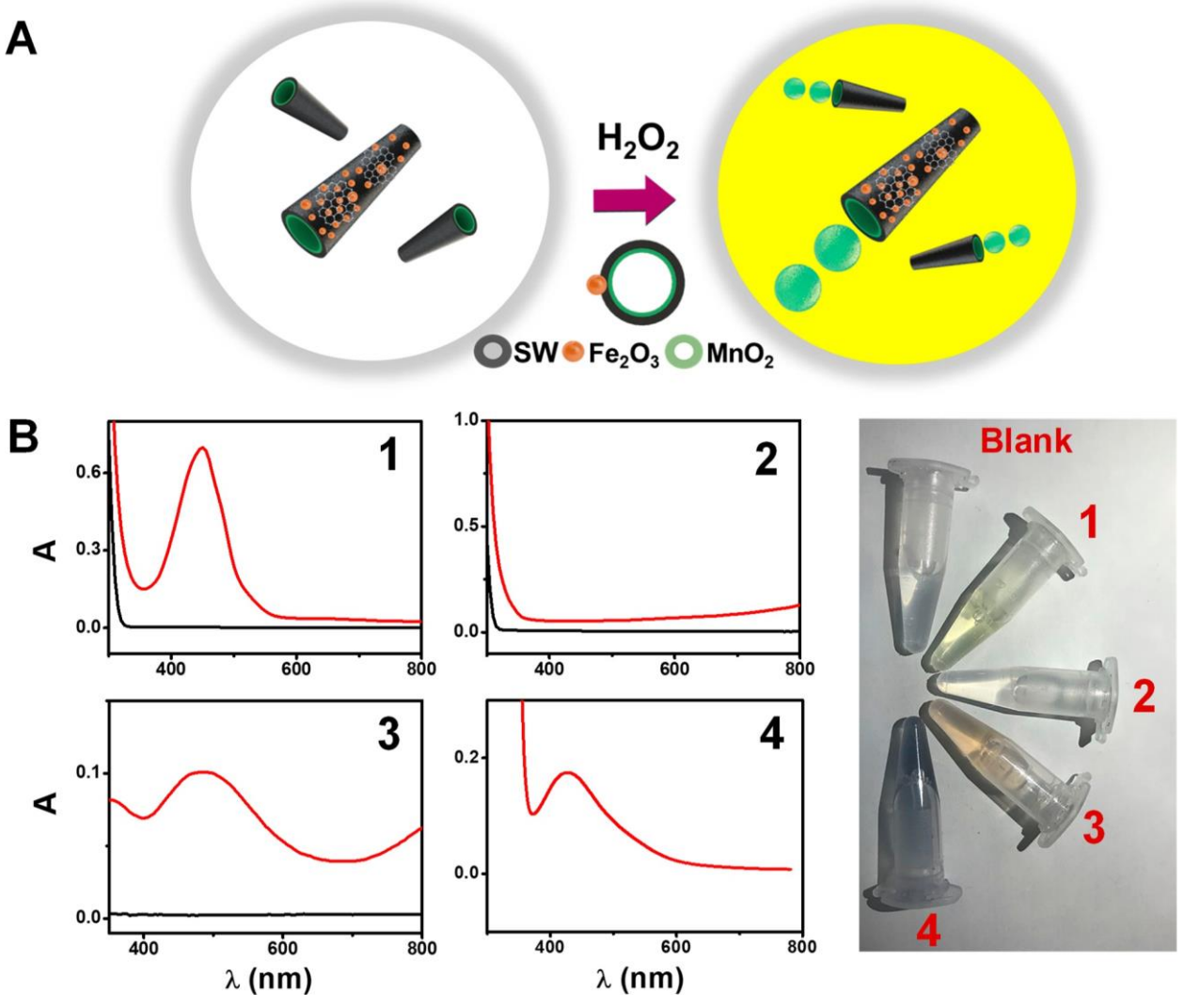

Figure 1. (A) Schematic of the colorimetric assay with SW−Fe_2O_3/MnO_2 micromotors for phenylenediamines detection. (B) UV−vis spectra of phenylenediamines isomers before (black line) and after (red line) treatment with SW−Fe_2O_3/MnO_2 micromotors in water and corresponding colors: (1) OPD, (2) MPD, (3) PPD, (4) OPD, MPD and PPD (conditions: 5% H_2O_2, 0.5% Tween 20, 30 min, 500 μM OPD, PPD, or MPD).

EXPERIMENTAL SECTION

Reagents and Materials. Carboxylic acid functionalized single-walled carbon nanotubes (SWCNTs−COOH, 0.7−1.3 nm diameter, cat. 704113), iron(III) oxide (nanopowder, <50 nm particle size, cat. 544884), 3,4-ethylenedioxythiophene (EDOT, cat. 483028), poly(sodium 4-styrenesulfonate) (PSS, cat. 243051), manganese(II) acetate tetrahydrate (cat. 229776), sodium sulfate (cat. 204447), Tween 20 (cat. P9416), hydrogen peroxide (cat. 216763), 2,2′-azino-bis(3-ethylbenzothiazoline-6-sulfonic acid) diammonium salt, ABTS (cat. A1888), *o*-phenylenediamine (cat. P9029), *m*-phenylenediamine (cat. P23954), *p*-phenylenediamine (cat. P6001), ferric chloride (cat. F7134), L-valine (cat. V0500), L-tyrosine (cat. 93829), aniline (cat. 242284), copper(II) (cat. 38996), and ascorbic acid (cat. 795437) were obtained from Sigma-Aldrich (Germany). Calcium chloride (cat. 2083) was obtained from Merck (Germany). All solutions were prepared by dilution in ultrapure water, 18.2 MΩ, or sample solution.

Instrumentation. Micromotors synthesis was carried out using an Autolab PGSTAT 12 (Eco Chemie, Utrecht, The Netherlands). Scanning electron microscopy (SEM) and energy-dispersive X-ray spectroscopy (EDX) images were obtained with a Jeol JSM 6335F instrument using an acceleration voltage of 10 kV. Transmission electron microscopy (TEM) images were obtained with an EM10 ZEISS microscopy using an acceleration voltage of 60 kV. Micromotor movement and speed were tracked by using an

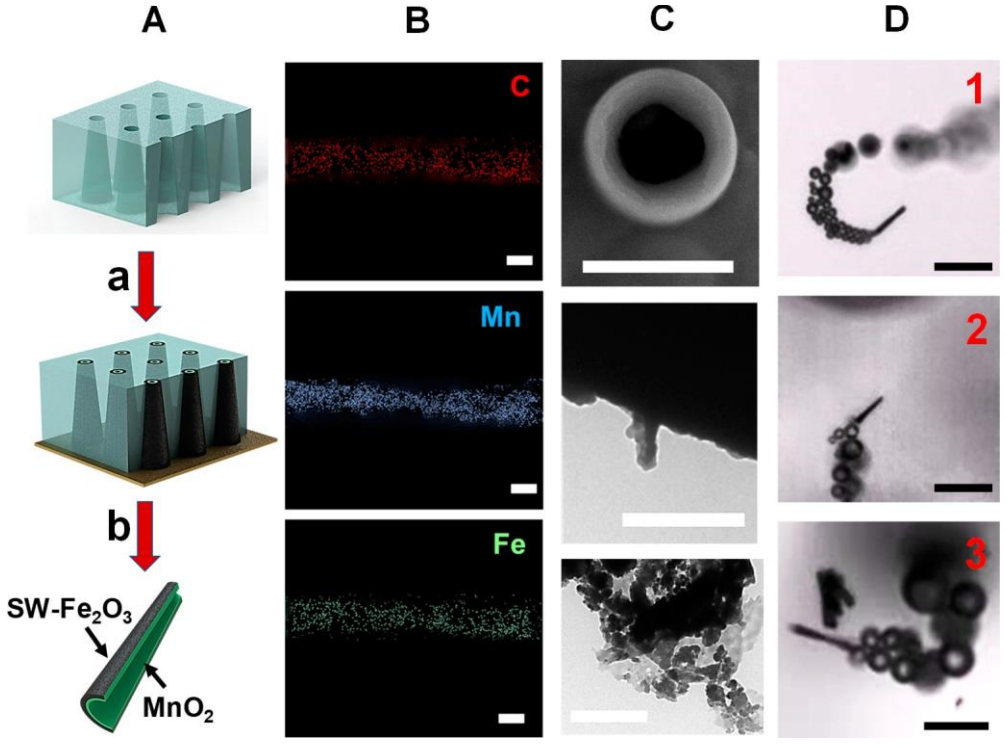

Figure 2. (A) Schematic of the fabrication of the SW−Fe_2O_3/MnO_2 tubular micromotors: (a) electrochemical deposition of the SW−Fe_2O_3 layer; (b) deposition of the catalytic MnO_2 layer. (B) Energy-dispersive X-ray mapping showing the distribution of C, Mn, and Fe in the micromotors. Scale bars, 2 μm. (C) Scanning and transmission electron microscopy images of a SW−Fe_2O_3/MnO_2 micromotor surface. Scale bars, 1 μm. (D) Time-lapse microscopy images (taken from Video S1) of the efficient propulsion of (1) SW−Fe_2O_3/MnO_2, (2) SW/MnO_2, and (3) PEDOT/MnO_2 micromotors in water (5% H_2O_2, 0.5% Tween 20). Scale bars, 10 μm.

inverted optical microscope (Nikon Eclipse Instrument Inc. Ti-S/L100), coupled with 20× objectives, and a Photometrics QuantEM 512/SC (Roper Scientific, Duluth, GA). UV−vis experiments were carried out using a PerkinElmer Lambda 20 spectrophotometer.

Micromotors Synthesis. SW−Fe_2O_3/MnO_2, SW/MnO_2, and PEDOT/MnO_2 micromotors were prepared by electrochemical deposition of the materials into the 2 μm diameter conical pores of a gold-sputtered polycarbonate membrane (cat. no. 70602511; Whatman, New Jersey, U.S.A.). For SW−Fe_2O_3/MnO_2 micromotors, simultaneous electrochemical reduction−deposition and nanoparticles entrapment was carried out using cyclic voltammetry (CV, over +0.3 to −1.5 V vs Ag/AgCl, 3 M, at 50 mV s^{-1}, for 10 cycles) from a platting solution containing 0.1 mg mL^{-1} of the nanotubes, 5 mg mL^{-1} of Fe_2O_3, and 0.5 M of Na_2SO_4 in 0.1 M H_2SO_4. Next, the inner catalytic MnO_2 layer was deposited by amperometry at 0.75 V for 1.3 C from aqueous solution containing 0.01 M manganese(II) acetate tetrahydrate. For SW/MnO_2 micromotors, the same conditions were used but obviating Fe_2O_3 nanoparticles addition in the platting solution. PEDOT/MnO_2 microtubes were electropolymerized at 0.80 V using a charge of 2 C from a 15 mL plating solution containing 10 mM EDOT and 125 mM PSS, followed by platting of the MnO_2 layer. In all cases, the sputtered gold layer was removed by hand-polishing and the micromotors were released from the membrane by sequential treatment with methylene chloride (30 min, two times), isopropyl alcohol, ethanol, and ultrapure water (18.2 Ω cm), with 3 min of centrifugation following each wash.

Micromotor Propulsion Experiments. To evaluate the speed of the micromotors in water media, a glass slide was placed on top of the microscope objective, and then 1 μL of each sample (tap water), surfactant (Tween 20), and H_2O_2 solutions was dropped onto the glass slide. To avoid sample dilution, the different solutions were prepared in tap water. Video acquisition was started 30 s after peroxide addition. NIS element software was used to track the speed of the micromotors under the different conditions.

Measurement of Peroxidase Activity of Micromotors. The peroxidase activity of micromotors was measured by using a chromogen, 2,2′-azino-bis(3-ethylbenzthiazoline-6-sulfonate) (ABTS). ABTS is water-soluble and has a strong absorption at a wavelength of 340 nm with a molar extinction coefficient ε_{340} of 3.66×10^4 M^{-1} cm^{-1}. On oxidation, ABTS forms a stable blue-green product presumed to be the cation radical, $ABTS^{+\bullet}$, which can be conveniently followed at λ_{max} at 415 nm (ε_{415} = 3.6×10^4 M^{-1} cm^{-1}). Experiments were carried out by mixing ABTS with hydrogen peroxide and micromotors solution to obtain a final concentration of 0.25 mM, 5 mM, and ∼110 000 micromotors/mL in acetate buffer solution (0.025 M, pH 4), respectively. The absorbance was recorded during 300 s at a wavelength of 415 nm. A similar procedure was employed to determined enzymatic parameters of catalysts employed using different ABTS substrate concentrations.

Colorimetric Discrimination of OPD, MPD, and PPD. Phenylenediamine isomers detection was performed by mixing in Eppendorf vials the different phenylenediamine solutions (25−1000 μM for OPD, 25−1000 μM for PPD, and 0.5−100 mM for MPD) with 5% H_2O_2, 0.5% Tween 20, and ∼110000 micromotors/mL. Then, 800 μL of supernatant was collected

after 15 min of micromotor's navigation and the absorbance spectrum was recorded between 350 and 800 nm at a scan speed of 240 nm min^{-1} and a slit of 1 nm.

RESULTS AND DISCUSSION

Figure 1 illustrates the overall strategy followed for OPD, PPD, and MPD individual detection with SW−Fe_2O_3/MnO_2 micromotors. As can be seen, initially not colored, OPD and PPD solutions (500 μM) exhibit strong yellow and pink color, respectively, after 30 min of micromotor's navigation under the presence of 5% H_2O_2. Blue color was observed when using an equimolar mixture of OPD and PPD. In contrast, no obvious color change was observed in the presence of MPD below a concentration of 50 mM. Such change in color might be attributed to the oxidation and dimerization of phenylenediamine isomers by hydroxyl radicals (•OH) released during peroxide decomposition in the catalytic MnO_2 layer.[49] Figure S1 illustrates the possible mechanism for the oxidation of phenylenediamine isomers. As can be seen, isomers are oxidized by •OH radicals via electron exchange and tend to polymerize to generate corresponding colors. In the case of MPD, the polymerization products do not exhibit accessible n−π* or π−π* transitions in the VIS region for convenient colorimetric detection. At higher MPD concentrations (>50 mM) overpolymerization occurs, and a black solution is formed.

Figure 2A illustrates the preparation of SW−Fe_2O_3/MnO_2 tubular micromotors.[38] For control experiments, SW/MnO_2 and PEDOT/MnO_2 micromotors were prepared in a similar fashion. Briefly, 2 μm cyclopore carbonate membranes were adopted as templates for the synthesis of ∼12 μm long conical micromotors. The preparation protocol relies on the simultaneous electrodeposition of the SW carbon outer layer along with the simultaneous entrapment of Fe_2O_3 nanoparticles. During the electrochemical reduction, the initial structure of SW nanotubes is partially modified resulting in the removal of oxygen functionalities, increasing thus the density of sp^2 carbons and overall hydrophobicity of the nanotubes, which tend to aggregate between them via π−π interactions, trapping the Fe_2O_3 nanoparticles present in the plating solution. Finally, the resulting structures tend to deposit within the walls of the membrane by hydrophobic interactions.[41,50] The deposition of the second MnO_2 layer essential for efficient micromotor propulsion and •OH radicals generation by peroxidase activity toward phenylenediamines isomers detection. The resulting micromotors were characterized by SEM, TEM, and EDX (Figure 2, parts B and C), further confirming the presence and uniform distribution of C, Mn and Fe within the conical micromotors and the presence of Fe_2O_3 particles on the outer surface. Figure 2D presents time-lapse images of the different micromotors swimming in a water solution (see Video S1). SW−Fe_2O_3/MnO_2 micromotors exhibit the greater speeds of 910 ± 150 μm s^{-1} (n = 12) due to the rough surface of the carbon nanomaterial and ferrite particles. SW/MnO_2 presents similar speeds of 780 ± 130 μm s^{-1} (n = 12), whereas PEDOT/MnO_2 exhibits the lower speeds of 185 ± 35 μm s^{-1} (n = 12) due to its smooth surface. Yet, as will be demonstrated in the following paragraphs, the incorporation of Fe_2O_3 nanoparticles imparts the micromotors with reusability properties and increases the overall analytical sensitivity for isomers detection.

Peroxidase-like activity of SW−Fe_2O_3/MnO_2, SW/MnO_2, and PEDOT/MnO_2 micromotors was evaluated based on the H_2O_2-mediated oxidation of a common substrate ABTS (for further details, see the Experimental Section). As shown in Figure S2, there is a clear absorption band which has a maximum absorbance at 415 nm, which correlates well with the characteristic absorption peak oxidation product of ABTS.[51] Also, the solution displays a typical green color in the presence of the micromotors (Figure S2, inset, Supporting Information). These observations illustrated that MnO_2 micromotors exhibit an intrinsic peroxidase-like activity. Figure 3A shows the absorbance evolution at 415 nm over time of

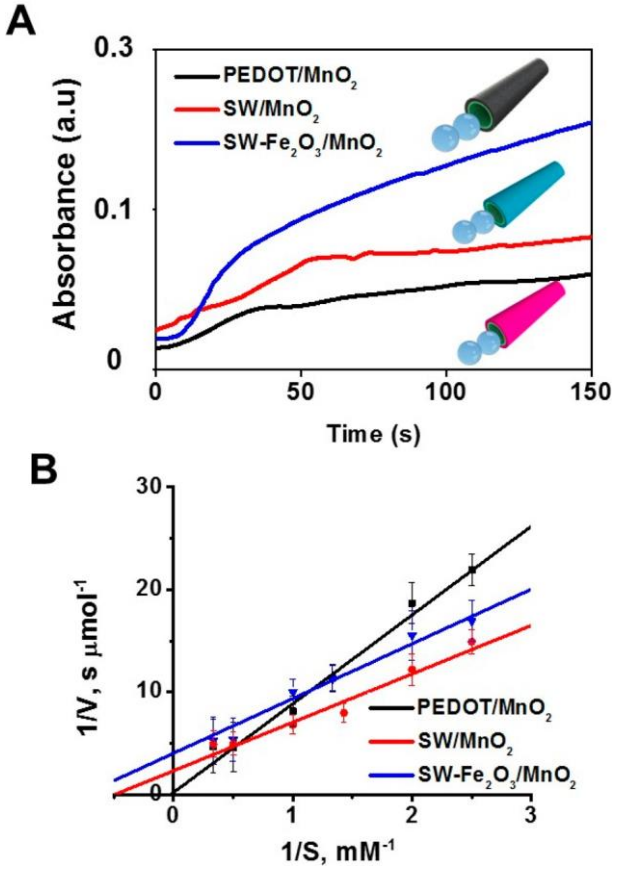

Figure 3. (A) Peroxidase-like activity of SW−Fe_2O_3/MnO_2, SW/MnO_2, and PEDOT/MnO_2 tubular static micromotors. ABTS oxidation product absorbance (λ = 415 nm) evolution with time for ∼110 000 micromotors/mL, 5 mM H_2O_2, and 0.25 mM ABTS in acetate buffer pH 4. (B) Lineweaver−Burk plot of SW−Fe_2O_3/MnO_2, SW/MnO_2, and PEDOT/MnO_2 tubular static micromotors (ABTS concentration from 0.2 to 3.0 mM, ∼110 000 micromotors/mL, and 5 mM H_2O_2 in acetate buffer pH 4). Error bars represent the standard deviation of three measurements.

ABTS solution (0.25 mM) with hydrogen peroxide (5 mM) and ∼110 000 micromotors/mL. As can be seen, micromotors with rough surface counterparts (SW−Fe_2O_3/MnO_2 and SW/MnO_2) exhibit higher peroxidase-like activity than smoother ones (PEDOT/MnO_2). A greater amount of $ABTS^{+\bullet}$ production is obtained when SW−Fe_2O_3/MnO_2 is used. This increment in $ABTS^{+\bullet}$ production could be only attributed to the presence of Fe_2O_3 particles in the micromotor. Note that the concentration of peroxide used in these experiments (5 mM) is insufficient for the micromotors to move, thus

eliminating mixing by agitation produced by micromotors self-propulsion. Apparent steady-state kinetic parameters for each micromotor system are listed in Table 1. Typical Michaelis−

Table 1. Apparent Steady-State Kinetic Parameters for Peroxidase-Like Micromotors

catalyst	K_m (mM)	V_{max} (μmol s^{-1})
PEDOT/MnO_2	4.6 ± 0.2	0.6 ± 0.2
SW/MnO_2	1.7 ± 0.1	0.3 ± 0.1
SW−Fe_2O_3/MnO_2	1.5 ± 0.1	0.3 ± 0.1
HRP[a]	3.7	

[a]Ref 50.

Menten curves were obtained by changing the concentration of ABTS. The Michaelis−Menten constant (K_m) and maximum initial velocity (V_{max}) were obtained using a Lineweaver−Burk plot (Figure 3B). The apparent K_m values for SW/MnO_2 and SW−Fe_2O_3/MnO_2 micromotors with ABTS as the substrate were lower than those of HRP,[52] which suggested that SW/MnO_2 and SW−Fe_2O_3/MnO_2 micromotors had higher affinity for ABTS than HRP. Such data reveals the enhanced properties of our micromotors over enzymatic approaches for phenylenediamines isomers detection. Surprisingly, V_{max} values (which indicate the number of substrate molecules converted into product by an enzyme molecule in a unit time when the enzyme is fully saturated with substrate) are 2 times higher for PEDOT/MnO_2 micromotors than for SW- and Fe_2O_3-based micromotors. Yet, the higher affinity of the substrate in SW−Fe_2O_3/MnO_2 micromotors enhances the sensitivity at low concentrations where the enzyme is not working in saturated conditions toward lower limits of detection (LODs).

Prior OPD and PPD detection and in order to get the best analytical performance, important variables such as time and number of micromotors were optimized (see Figure 4). Since MPD does not display any apparent color in working conditions, such compound was not included in optimization studies. Micromotors concentration was estimated by counting the micromotors in a limited well-defined area on the microscope and extrapolating to a drop area corresponding to a 1 μL of solution. This procedure was performed three times, and data was presented as an average micromotor concentration. As can be seen, a concentration ∼14 000 ± 2000 micromotors/mL produce lower signal for OPD and PPD at a reaction time of 20 min. Signals for both analytes increase as micromotors concentrations increase to ∼28 000 ± 4000 and ∼55 000 ± 7000 micromotors/mL (data not shown). Maximum signal for both analytes is reached at a concentration of ∼110 000 (±10 000) micromotors/mL, and then remains constant. Thus, the later number (concentration) of micromotors was chosen for subsequent assays. Figure 4B shows the optimization of reaction time. As can be seen, the maximum signal was achieved at reaction time of 15 min, and then remained constant. Reaction times higher than ∼1 h produce black solutions with absorbance in all visible spectra that did not allow phenylenediamines discrimination due to overpolymerization of the analytes in the solution. Moreover, several control experiments were made to ensure the suitability of the SW−Fe_2O_3/MnO_2 micromotors for the intended application. As can be seen in Figure 4C, higher dimerization signals of OPD and PPD were obtained for swimming SW−Fe_2O_3/MnO_2 (g) due to their higher peroxidase-like activity and their greater speed movement that enhances solution

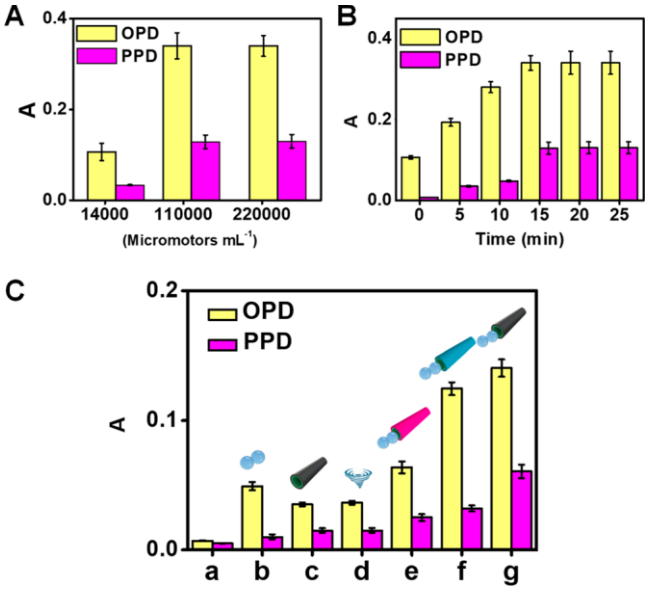

Figure 4. (A) Micromotor concentration and (B) assay time reaction optimization (SW−Fe_2O_3/MnO_2 micromotors, 5% H_2O_2, Tween 0.5%, 500 μM OPD or 300 μM PPD). (C) Control experiments for OPD and PPD detection (200 μM) with (a) OPD and PPD without H_2O_2 and micromotors, (b) with H_2O_2, (c) with SW−Fe_2O_3/MnO_2 micromotors, (d) with stirring SW−Fe_2O_3/MnO_2, (e) with PEDOT/MnO_2 and H_2O_2, (f) with SW/MnO_2 and H_2O_2, and (g) SW−Fe_2O_3/MnO_2 and H_2O_2.

mixing versus SW/MnO_2 (f) and PEDOT/MnO_2 (e) micromotors. Other experiments reveal the need for OH radical generation (a−d), where no significant signals are obtained due to the absence of hydrogen peroxide or peroxidase-like catalyst activity.

Calibration curves were obtained using the optimized conditions (5% H_2O_2, 0.5% Tween 20, ∼110 000 micromotors/mL and a reaction time of 15 min) within the concentration range of 25−1000 μM. Figure 5 shows calibration UV−vis spectra of different micromotors-treated contaminated solutions and corresponding calibration curves fits for OPD (A) and PPD (B) in ultrapure water and in tap water. As can be seen, both calibrations curves (in ultrapure and tap water) exhibit a similar sensitivity, which testifies to the absence of matrix effects for both OPD and PPD. An LOD and limit of quantitation (LOQ) of 5 and 16.7 μM, respectively, were obtained for OPD, with linear range between 16.7 and 500 μM. An LOD and LOQ of 6 and 20 μM, respectively, were obtained for PPD and a linear range between 20 and 300 μM. In a similar procedure using Fe_3O_4/nitrogen-doped graphene quantum dots, lower LODs of 230 and 530 nM were reported in the colorimetric detection of OPD and PPD.[9] Yet, the LD_{50} (concentration that kills 50% of cells in a cell culture) is 110 and 20 μM for OPD and PPD, respectively,[53] so SW−Fe_2O_3/MnO_2 micromotors can be applied to detect toxic doses of OPD and PPD in water samples with enough sensitivity in just 15 min without matrix interferences in typical water samples. In addition, our micromotor-based strategy allow for a drastic reduction of analysis time (i.e., 15 min) as compared with the 30 min required using static nanoparticles[9] and reusability toward repeated measurements without additional centrifugation or washing steps.

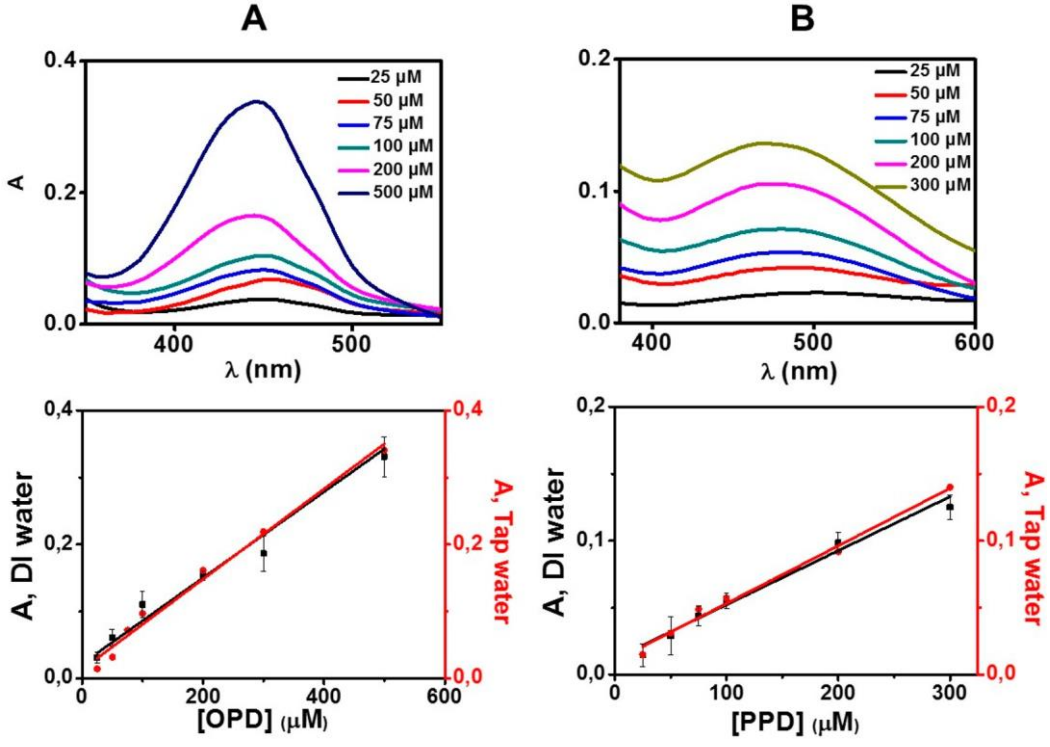

Figure 5. (A) OPD calibration spectra in ultrapure water and calibrations curves in ultrapure water and tap water. (B) PPD calibration spectra in ultrapure water and calibrations curves in ultrapure water and tap water. (Conditions: 5% H_2O_2; 0.5% Tween 20; SW−Fe_2O_3/MnO_2 micromotors ~110 000 micromotors/mL; reaction time of 15 min). Errors bars represent the standard deviation of three measurements.

The selectivity of our sensing protocol was evaluated by performing the assay under the presence of high concentrations of metal cations and other organic compounds typically found in water samples. Figure 6 shows an interference/selectivity summary expressed as ΔA(%) (% absorbance variation of a treated solution with the interference regarding the assay without interference) (assay conditions: SW−Fe_2O_3/MnO_2, ~110 000 micromotors/mL, 5% H_2O_2, 0.5 % Tween 20). As can be seen, Ca^{2+}, aniline, tyrosine, ascorbic acid, and valine did not interfere in OPD and PPD determination at the concentration levels assayed (100, 10, 10, 10, 100 mM, respectively). Transition metal cations as Cu^{2+} and Fe^{3+} could interference (ΔA (%) is 15% and 35%, respectively) in OPD and PPD determination in extremely high concentrations, which are not normally present in water samples (>20 µM).

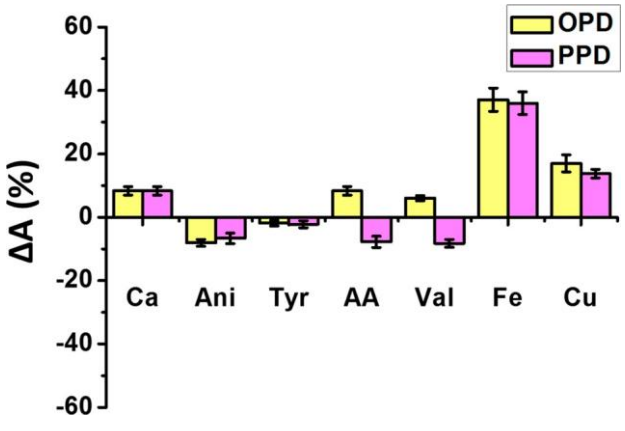

Figure 6. Interference of Ca^{2+}, aniline, tyrosine, ascorbic acid, valine, Fe^{3+}, and Cu^{2+} at a level of 100, 10, 1, 10, 100, 0.02, 0.02 mM.
(Conditions: 5% H_2O_2; 0.5% Tween 20, ~110 000 SW−Fe_2O_3/MnO_2 micromotors/mL; reaction time of 15 min; 100 µM OPD or PPD).

Finally, SW−Fe_2O_3/MnO_2 micromotors were employed to determine OPD and PPD in tap water samples spiked with 25 and 100 µM of each compound. Percent recoveries (~100%) were obtained in both samples, which testifies to the applicability of our method for practical water samples sensing. Finally, SW−Fe_2O_3/MnO_2 micromotors reusability was studied by eliminating the supernatant after the assay while the micromotors were trapped by a magnet at the bottom of the Eppendorf vial taking advantage of the magnetic properties of Fe_2O_3 particles. Then, new reagents were put on the Eppendorf vial to repeat the assay. As can be seen in Figure 7, OPD and PPD signals were obtained according to calibration curves and SW−Fe_2O_3/MnO_2 micromotors could be reused for further assays.

CONCLUSIONS

We have demonstrated the use of a hybrid SW−Fe_2O_3 micromotor with an inner MnO_2 catalytic layer for phenylenediamines detection (OPD and PPD) in a simple colorimetric assay in just only 15 min. Catalytic decomposition of H_2O_2 fuel by the inner MnO_2 catalytic layer results in the production of oxygen bubbles along with hydroxyl radicals for analytes dimerization. The combination of Fe_2O_3 nanoparticles along with the irregular SW backbone imparts the micromotors with reusability properties and assists the OH radical production rate, increasing thus the overall analytical sensitivity (i.e., more color generation) when compared with SW or smooth PEDOT counterparts. Compared with previously

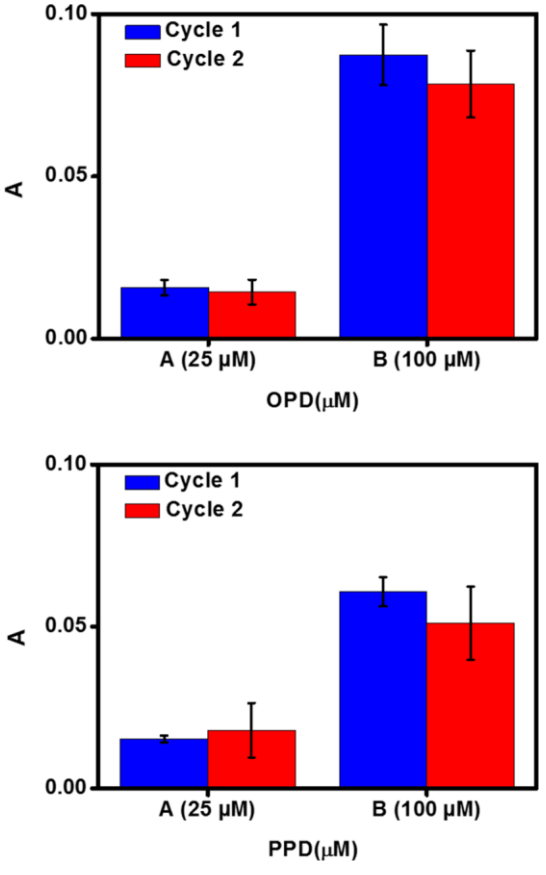

Figure 7. OPD and PPD determination in tap water samples and reusability of the micromotors (Conditions: 5% H_2O_2; 0.5% Tween 20, ~110 000 SW−Fe_2O_3/MnO_2 micromotors/mL; reaction time of 15 min).

reported procedures using static artificial enzyme nanoparticles,[9,17−20] the use of our moving micromotors allows for a drastic reduction of the analysis time and reusability without any additional centrifugation or washing steps. Moreover, the practical utility of our micromotors has been demonstrated for OPD and PPD detection in water samples without matrix interferences. Enhanced micromotor movement along with radical generation results in rapid and sensitive OPD and PPD detection with an LOQ and linear range suitable for analytes quantification according of their aquatic toxicity (LD_{50}: 110 and 20 μM, respectively). Besides, SW−Fe_2O_3/MnO_2 micromotors could be reusable for repetitive assays. All in all, SW−Fe_2O_3/MnO_2 micromotors demonstrate the potential future of micromotors for further sensing

ASSOCIATED CONTENT

Supporting Information

The Supporting Information is available free of charge on the ACS Publications website at DOI: XXX

Phenylene isomers dimerization mechanism and UV−vis spectrum of ABTS after reaction with SW−Fe_2O_3/ MnO_2 micromotors (PDF) Efficient propulsion of SW−Fe_2O_3/MnO_2, SW/MnO_2, and PEDOT/MnO_2 micromotors in water (AVI)

AUTHOR INFORMATION

Corresponding Authors

*E-mail: beatriz.jurado@uah.es.

*E-mail: alberto.escarpa@uah.es.

ORCID

Beatriz Jurado-Sánchez: 0000-0002-6584-1949

Alberto Escarpa: 0000-0002-7302-0948

Author Contributions

The manuscript was written through contributions of all authors. All authors have given approval to the final version of the manuscript.

Notes

The authors declare no competing financial interest.

ACKNOWLEDGMENTS

R.M.-H. acknowledges the FPI fellowship received from the Spanish Ministry of Economy and Competitiveness (BES- 2015-072346). B.J.-S. acknowledges support from the Spanish Ministry of Economy and Competitiveness (RYC-2015-17558, co-financed by the EU) and from the University of Alcalá (Proyectos para la Creacion y Consolidacion de Grupos, Plan Propio UAH, CCGP2017-351 EXP/040). A.E. acknowledges financial support from the Spanish Ministry of Economy and Competitiveness (CTQ2014-58643-R and CTQ2017-86441- C2-1-R) and the NANOAVANSENS program (S2013/MIT- 3029) from the Community of Madrid.

REFERENCES

(1) Pinheiro-Sant'Ana, H. M.; Guinazi, M.; Oliveira, D. D. S.; Della Lucia, C. M.; Reis, B. D. L.; Brandão, S. C. C. *J. Chromatogr. A* 2011, *1218*, 8496.

(2) Wang, H.-F.; Wu, Y.-Y.; Yan, X.-P. *Anal. Chem.* 2013, *85*, 1920.

(3) Mauri-Aucejo, A. R.; Ponce-Catala,P.; Belenguer-Sapiña, C.; Amoros, P. *Talanta* 2015, *134*, 560.

(4) Samanta, S.; Kar, C.; Das, G. *Anal. Chem.* 2015, *87*, 9002.

(5) Jansson, E. T. *J. Sep Sci.* 2018, *41*, 385.

(6) Gichner, T.; Stavreva, D. A.; Van Breusegem, F. *Mutat. Res., Genet. Toxicol. Environ. Mutagen.* 2001, *495*, 117.

(7) Ngamdee, K.; Martwiset, S.; Tuntulani, T.; Ngeontae, W. *Sens. Actuators, B* 2012, *173*, 682.

(8) Li, N.; Gu, Y.; Gao, M.; Wang, Z.; Xiao, D.; Li, Y.; Lin, R.; He, H. *Spectrochim. Acta, Part A* 2015, *140*, 328.

(9) Shi, B.; Su, J.; Zhang, L.; Huang, M.; Li, X.; Zhao, S. *Nanoscale* 2016, *8*, 10814.

(10) Tokuda, H.; Kimura, Y.; Takano, S. *J. Chromatogr A* 1986, *367*, 345.

(11) Wang, P. G.; Krynitsky, A. J. *J. Chromatogr. B: Anal. Technol. Biomed. Life Sci.* 2011, *879*, 1795.

(12) Wang, S.-P.; Huang, T.-H. *Anal. Chim. Acta* 2005, *534*, 207.

(13) Dobberstein, P.; Korte, E.; Meyerhoff, G.; Pesch, R. *Int. J. Mass Spectrom. Ion Phys.* 1983, *46*, 185.

(14) Dong, S.; Chi, L.; Zhang, S.; He, P.; Wang, Q.; Fang, Y. *Anal. Bioanal. Chem.* 2008, *391*, 653.

(15) Wang, J.; Cao, Y.; Xu, Y.; Li, G. *Biosens. Bioelectron.* 2009, *25*, 532.

(16) Gao, L. Z.; Zhuang, J.; Nie, L.; Zhang, J. B.; Zhang, Y.; Gu, N.; Wang, T. H.; Feng, J.; Yang, D. L.; Perrett, S.; Yan, X. *Nat. Nanotechnol.* 2007, *2*, 577.

(17) Asati, A.; Santra, S.; Kaittanis, C.; Nath, S.; Perez, J. M. *Angew. Chem., Int. Ed.* 2009, *48*, 2308.

(18) Chen, W.; Chen, J.; Liu, A. L.; Wang, L. M.; Li, G. W.; Lin, X. H. *ChemCatChem* 2011, *3*, 1151.

(19) Mu, J.; Wang, Y.; Zhao, M.; Zhang, L. *Chem. Commun.* 2012, *48*, 2540.

(20) Liu, X.; Wang, Q.; Zhao, H.; Zhang, L.; Su, Y.; Lv, Y. *Analyst* 2012, *137*, 4552.
(21) He, W.; Wamer, W.; Xia, Q.; Yin, J.-J.; Fu, P. P. *J. Environ. Sci. Health, Part C* 2014, *32*, 186.
(22) Ozin, G. A.; Manners, I.; Fournier-Bidoz, S.; Arsenault, A. *Adv. Mater.* 2005, *17*, 3011.
(23) Solovev, A. A.; Mei, Y.; Bermúdez Ureña, E.; Huang, G.; Schmidt, O. G. *Small* 2009, *5*, 1688.
(24) Wang, H.; Pumera, M. *Chem. Rev.* 2015, *115*, 8704.
(25) Ebbens, S. J.; Howse, J. R. *Soft Matter* 2010, *6*, 726.
(26) Wang, H.; Pumera, M. *Adv. Funct. Mater.* 2018, 1705421.
(27) Mei, Y.; Solovev, A. A.; Sanchez, S.; Schmidt, O. G. *Chem. Soc. Rev.* 2011, *40*, 2109.
(28) Sengupta, S.; Ibele, M. E.; Sen, A. *Angew. Chem., Int. Ed.* 2012, *51*, 8434.
(29) Wang, W.; Chiang, T. Y.; Velegol, D.; Mallouk, T. E. *J. Am. Chem. Soc.* 2013, *135*, 10557.
(30) Wang, J. *Nanomachines: Fundamentals and Applications*; Wiley: Weinheim, Germany, 2013.
(31) Jurado-Sánchez, B.; Pacheco, M.; Maria-Hormigos, R.; Escarpa, A. *Appl. Mater. Today* 2017, *9*, 407.
(32) Kim, K.; Guo, J.; Xu, X.; Fan, D. L. *Small* 2015, *11*, 4037.
(33) Karshalev, E.; Esteban-Fernandez de Avila, B.; Wang, J. *J. Am. Chem. Soc.* 2018, *140*, 3810.
(34) Wang, J. *Biosens. Bioelectron.* 2016, *76*, 234.
(35) Jurado-Sanchez, B.; Pacheco, M.; Rojo, J.; Escarpa, A. *Angew. Chem., Int. Ed.* 2017, *56*, 6957.
(36) Esteban-Fernández de Avila, B.; Lopez-Ramirez, M. A.; Baé, D.; Jodra, A.; Singh, V. V.; Kaufmann, K.; Wang, J. *ACS Sens* 2016, *1*, 217.
(37) Pacheco, M.; Jurado-Sanchez, B.; Escarpa, A. *Anal. Chem.* 2018, *90*, 2912.
(38) Jurado-Sanchez, B.; Escarpa, A.; Wang, J. *Chem. Commun.* 2015, *51*, 14088.
(39) Cinti, S.; Valdes-Ramirez, G.; Gao, W.; Li, X.; Palleschi, G.; Wang, J. *Chem. Commun.* 2015, *51*, 8668.
(40) Rojas, D.; Jurado-Sánchez, B.; Escarpa, A. *Anal. Chem.* 2016, *88*, 4153.
(41) Ye, H.; Ma, G.; Kang, J.; Sun, H.; Wang, S. *Chem. Commun.* 2018, *54*, 4653.
(42) Feng, X.; Zhang, Y.; Li, Y.; Huang, Z.; Chen, S.; Ma, Y.; Zhang, L.; Wang, L.; Yan, X. *Chem. Lett.* 2015, *44*, 399.
(43) Maria-Hormigos, R.; Jurado-Sanchez, B.; Vazquez, L.; Escarpa, A. *Chem. Mater.* 2016, *28*, 8962.
(44) Ye, H.; Sun, H.; Wang, S. *Chem. Eng. J.* 2017, *324*, 251.
(45) Wang, H.; Zhao, G.; Pumera, M. *J. Am. Chem. Soc.* 2014, *136*, 2719.
(46) Safdar, M.; Wani, O. M.; Janis, J. *ACS Appl. Mater. Interfaces* 2015, *7*, 25580.
(47) Teo, W. Z.; Wang, H.; Pumera, M. *Chem. Commun.* 2016,*52*, 4333.
(48) Chen, X. Z.; Hoop, M.; Mushtaq, F.; Siringil, E.; Hu, C.; Nelson, B. J.; Pané, S. *Appl. Mater. Today* 2017, *9*, 37.
(49) He, Z.; Lin, L.; Song, S.; Xia, M.; Xu, L.; Ying, H.; Chen, J. *Sep. Purif. Technol.* 2008, *62*, 376.
(50) Wu, K.; Hu, S. *Carbon* 2004, *42*, 3237.
(51) Re, R.; Pellegrini, N.; Proteggente, A.; Pannala, A.; Yang, M.; Rice-Evans, C. *Free Radical Biol. Med.* 1999, *26*, 1231.
(52) Ozaki, S. I.; Ortiz de Montellano, P. R. *J. Am. Chem. Soc.* 1995, *117*, 7056.
(53) Bajot, F.; Cronin, M. T. D.; Roberts, D. W.; Schultz, T. W. *SAR QSAR Environ. Res.* 2011, *22*, 51.